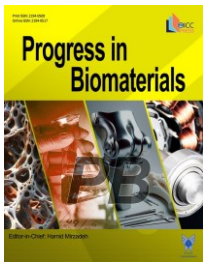

Volume 14, Issue 4, 2025: Article 17

Progress in Biomaterials (PIBM)

https://doi.org/10.57647/pibm.2025.1403.18

# Bioactive Photo-crosslinkable GelMA Hydrogel Incorporating Metal Oxide Nanoparticles for Bone Tissue Regeneration

Lígia Espoliar Corrêa[1], Ester Alves Ferreira Bordini[2], Vitor de Toledo Stuani[1], Larissa Álamo[1], Ruan Henrique Delmonica Barra[3], Erika Soares Bronze-Uhle[1], Laura Ferreira Almeida[1], Lídia de Oliveira Fernandes[4], Carolina Alves Andrade[1], Juliano Milanezi de Almeida[3], Carlos Alberto de Souza Costa[4], Diana Gabriela Soares[1*]

[1]*Department of Operative Dentistry, Endodontics and Dental Materials, Bauru School of Dentistry, University of São Paulo (USP), Alameda Dr. Octávio Pinheiro Brisolla, 9-75, Bauru, São Paulo, 17012-901, Brazil*
[2]*Department of Dental Materials and Prosthodontics, Ribeirão Preto School of Dentistry, University of São Paulo (USP), Av. do Café - Subsetor Oeste - 11 (N-11), Ribeirão Preto, São Paulo, 14040-904, Brazil*
[3]*Department of Diagnosis and Surgery, School of Dentistry of Araçatuba, São Paulo State University (Unesp), Street José Bonifácio, 1193 - Vila Mendonca, Araçatuba, São Paulo, 16015-050, Brazil*
[4]*Department of Physiology and Pathology, School of Dentistry of Araraquara, São Paulo State University (Unesp), Street Humaitá, 1680 - Araraquara, São Paulo, 14801-385, Brazil*

***Corresponding author:** dianasoares@fob.usp.br

**Original Research**

Received:
01 July 2025

Revised:
16 November 2025

Accepted:
30 December 2025

Published in Issue:
31 December 2025



**Abstract**

This study aimed to develop a photo-crosslinkable and 3D-printable biomaterial, comprising methacrylated gelatin (GelMA) functionalized with magnesium oxide (MgO) and silicon dioxide ($SiO_2$) nanoparticles, as a bioactive scaffold for bone regeneration. Cytocompatible concentrations of MgO and $SiO_2$ were identified using a dose-response assay, and selected formulations were characterized in terms of structural architecture, chemical composition, and cumulative nanoparticle release. Murine calvarial preosteoblasts were seeded onto hydrogels to evaluate long-term viability, proliferation, collagen expression, and mineralized matrix deposition. The formulations were also assessed for extrusion-based 3D printability. MgO and $SiO_2$ at 0.05% and 0.025% (w/v) were used, which positively modulated the GelMA porosity. No chemical modifications to GelMA were detected; instead, the nanoparticles were gradually released. Cell viability was maintained in all groups over 14 days, with enhanced proliferation observed from day 3 onward. All oxide-functionalized GelMA formulations showed increased collagen expression and calcium-rich matrix deposition, with the 0.05% group inducing the greatest mineralization at 14 days. Well-organized 3D-printed meshes were successfully obtained, demonstrating that the combination of bioactivity and high printability can be leveraged for the development of personalized bone therapies. GelMA containing 0.05% MgO and $SiO_2$ exhibited the highest osteogenic activity, representing the most promising platform for bone-tissue regeneration.

**Keywords:** GelMA, Magnesium, Silicon, Bone, Regeneration, 3D-print

**Cite this article:** Corrêa, L. E., Bordini, E. A. F., Stuani, V. D. T., Álamo, L., Delmonica, B. R. H., Bronze-Uhle, E. S., Almeida, L. F., Fernandes, L. D. O., Andrade, C. A., Almeida, J. M. D., Souza Costa, C. A. D., Soares, D. G., (2025). Bioactive Photo-crosslinkable GelMA Hydrogel Incorporating Metal Oxide Nanoparticles for Bone Tissue Regeneration, *Progress in Biomaterials,* 14(04), Article 17.
https://doi.org/10.57647/pibm.2025.1403.18

## Graphical abstract

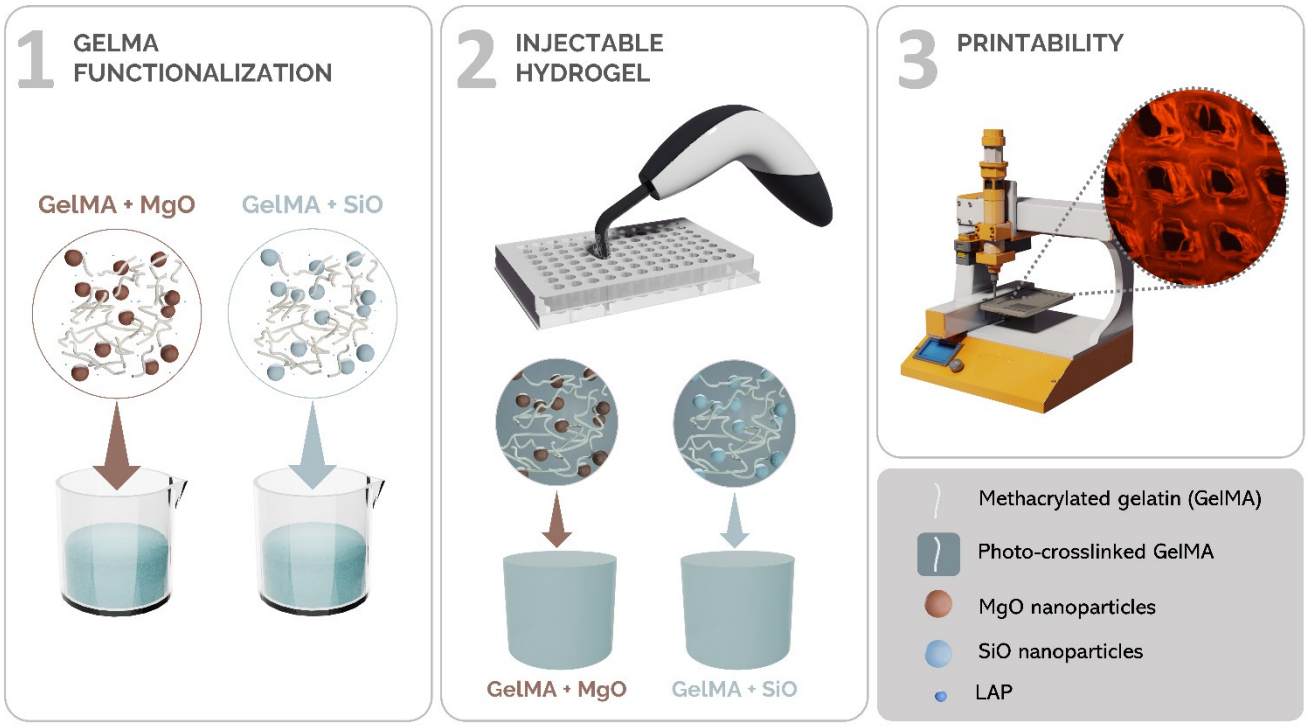


## 1. Introduction

Bone tissue loss is a clinically significant condition associated with various causes, such as trauma, systemic diseases, congenital anomalies, nutritional and hormonal deficiencies, cancer, and severe joint disorders [1; 2; 3; 4; 5]. In dentistry, this condition compromises oral structural stability, affecting mastication, speech, and facial aesthetics, which negatively affect patients' quality of life. Periodontal disease plays a fundamental role in alveolar bone destruction, which leads to tooth mobility, pain, and loss. These changes hinder prosthetic rehabilitation and increase the complexity of treatment, often requiring advanced procedures, such as bone grafting and tissue regeneration. While small bone defects may heal naturally, extensive bone loss, pathological fractures, and infections demand surgical intervention and the use of bone substitutes [4].

Autologous grafts, considered the gold standard for bone regeneration owing to their osteoconductive and osteoinductive properties, and rich vascularization, are effective, but limited by donor-site morbidity and availability. Alternatives include allogeneic, xenogeneic, and alloplastic materials, which have biological, structural, or ethical limitations [6; 7]. In oral and maxillofacial surgery, the choice of material depends on defect size, shape, and tissue viability. Common procedures involving bone grafts include dental implantation, ridge augmentation, sinus lifts, socket preservation, and periodontal surgery. Among these, xenografts, particularly those derived from bovine and porcine sources, have been successfully used because of their biomimetic composition that supports osteoconduction [6; 7].

Recently, biomaterials based on xenogeneic natural polymers, such as collagen, gelatin, and alginate, have been the focus of studies in the field of tissue engineering, with the aim of developing biomimetic tissue substitutes. Collagen is the primary component of the extracellular matrix (ECM) in most soft and hard tissues in animals and humans. Collagen networks play a dominant role in regulating cellular behavior by maintaining the extracellular microenvironment [8]. Although these polymers are excellent candidates for biomedical applications, their high degradability and low mechanical strength are the main challenges [9; 10; 11].

Methacrylation of natural polymers is a promising strategy for the development of biomimetic hydrogels, offering enhanced structural stability to biomaterials. This modification allows for the formulation of injectable and in situ photo-crosslinkable hydrogels, thereby extending the working time and enabling their use in 3D printing for the fabrication of xenogeneic grafts, expanding their range

10.57647/pibm.2025.1403.18

of clinical applications [12]. Among these, methacrylated gelatin (GelMA) has attracted considerable attention. Owing to the low degree of methacrylation (typically less than 5% methacrylic anhydride), key functional sites, such as Garginine-glycine-aspartic acid (RGD) motifs and matrix metalloproteinase (MMP)-sensitive sequences, are available for cell adhesion and enzymatic remodeling. Furthermore, as GelMA is primarily derived from denatured collagen, it closely mimics the structure of the native ECM, qualifying it as a biomimetic material. These GelMA properties support its use in the evaluation of bone, cartilage, muscle, and vascular tissue regeneration [13; 14; 15].

Magnesium oxide (MgO) and silicon dioxide (SiO2) nanoparticles have attracted increasing attention as bioactive additives in GelMA hydrogels, particularly for applications in bone and vascular regeneration. These oxides play key roles in promoting mesenchymal stem cell differentiation, and enhancing both osteogenic and angiogenic processes. Notably, MgO and SiO2 stimulate endothelial cells to produce nitric oxide through a mechanism similar to that of vascular endothelial growth factor (VEGF), thereby supporting neovascularization, an essential factor for the survival and integration of engineered tissues [16; 17; 18; 19]. When incorporated into GelMA hydrogels, these mineral nanoparticles improved the bioactivity and mechanical properties of the scaffold, making them more suitable for load-bearing applications in bone tissue engineering. Compared to traditional mineral phases, such as hydroxyapatite or beta-tricalcium phosphate, MgO and SiO2 nanoparticles exhibit superior dispersion within the GelMA network. This uniform distribution contributes to the creation of a favorable microenvironment for cellular adhesion, proliferation, and differentiation [20; 21]. Therefore, the present study aimed to perform a comprehensive screening of GelMA hydrogels enriched with MgO and SiO2 nanoparticles to identify the optimal composition of the biomaterial for bone tissue engineering applications.

## 2. Materials and methods

**Fabrication of the GelMA hydrogel:** Porcine type A gelatin (Sigma-Aldrich, St. Louis, MO, USA) was dissolved in phosphate-buffered saline (PBS; pH 7.4, Gibco, Invitrogen, Carlsbad, CA, USA) at 50°C (10% w/v). After dissolution, methacrylic anhydride (Sigma-Aldrich) was added dropwise to ensure complete emulsification. After stirring for 2 h, 100 mL of PBS (Gibco, Invitrogen) was added. The resulting solution was dialyzed in deionized water for 5 days, with the water replaced two to three times per day to remove any unreacted compounds. After the dialysis period, the solution was filtered through a 0.22-µm filter and frozen in 50 mL of Falcon-style flasks, with up to 40 mL per flask, at -80°C for 2 days. The frozen Falcon tubes were subjected to vacuum freeze-drying (Liotop, Liobras, São Carlos, Brazil) for 5 days. Once the freeze-drying process was complete, GelMA was stored at 20°C until use. Metacrylation was confirmed using Fourier-transform infrared (FTIR) spectroscopy (Supplemental Material, Figure S1).

GelMA hydrogel samples were obtained as previously described by [22]. In this procedure, the lyophilized, weighed, and sterilized GelMA at a concentration of 15% (w/v) was dissolved in PBS at 50°C. Lithium phenyl-2,4,6-trimethylbenzoylphosphinate (LAP, Sigma-Aldrich) was added to the solution at a weight ratio of 0.075. These parameters were selected because of the enhanced structural stability and better viability of the tested cell lines in previous studies [22]. The solution was vortexed until it was completely homogenized and then centrifuged for 5 min at 12,000 rpm to remove bubbles. Once prepared, the solution was injected into 96-well plates with 100 µL per sample. Photopolymerization was then performed for 30 s using an LED light with a wavelength range of 385–515 nm (1200 MW/cm ²; Bluephase N, Ivoclar-Vivadent, Buffalo, NY, USA). Finally, samples with a diameter of 7 mm and thickness of 2.5 mm were obtained.

**Oxides incorporation:** To improve the dispersion of oxides and prevent their aggregation within the GelMA network, a solution with a concentration of 5% (w/v) was prepared by dissolving MgO (Sigma-Aldrich; particle size < 50 nm) and SiO2 (Sigma-Aldrich; particle size: 5–20 nm) in Eppendorf tubes containing 970 µL of aqueous bovine serum albumin (BSA; 0.05% w/v, Sigma-Aldrich) and 30 µL of anhydrous ethanol (ETOH; Thermo Fisher Scientific, Waltham, MA, USA). The solution was subjected to vortexing for 1 min to ensure complete homogenization [23]. The oxides were diluted in PBS+LAP solution to obtain concentrations of 1%, 0.1%, 0.075%, 0.05%, and 0.025% (w/v), using the formula C1 × V1 = C2 × V2. These solutions were used to obtain the oxide-functionalized GelMA. To ensure accuracy, the final volumes after dissolution were measured and only a negligible change (<1%) was observed. These concentrations were initially established for biological screening to select biocompatible formulations. A pure GelMA hydrogel was used as a control.

**Hydrogel microarchitecture:** Samples were lyophilized at -52°C, mounted on metallic stubs, and sputter-coated

USA) at accelerating voltages of 10–15 kV, and magnifications of 250× and 500× (n = 2).

**Chemical composition:** FTIR was performed using an IR PRESTIGE-21 spectrometer (Shimadzu, Kyoto, Japan) equipped with an attenuated total reflectance (ATR) accessory. For each formulation, FTIR spectra were collected in ATR mode with 32 scans at a resolution of 4 $cm^{-1}$, covering the spectral range of 450–4000 $cm^{-1}$.

**Oxide release assay:** For the oxide release assay, hydrogel samples were prepared according to the same protocol described for the cell culture experiments and individually incubated in 200 µL of PBS at 37°C. At predetermined time points, 3 h, 15 h, 1 day, 3 days, 7 days, and 14 days, the samples were gently agitated for 30 s to ensure homogenization. Subsequently, 200 µL of the supernatant was collected from each tube, transferred to new microtubes, and stored at −20 °C for later analysis. Fresh PBS was added to each tube after collection to maintain a constant immersion volume. The concentration of the released oxides in the supernatants was quantified using UV-Vis spectrophotometry with the characteristic absorbance wavelengths of each oxide: 600 nm for MgO and 235 nm for SiO2. The cumulative release was calculated over time and expressed as a percentage of the total mass of each oxide initially incorporated into the hydrogel.

**Degradation assay:** Samples were prepared as previously described, placed in 48-well plates containing 1 mL of PBS (Sigma-Aldrich), with or without type I collagenase (1 U/mL; Sigma-Aldrich) [24], and incubated for 24 h at 37°C to allow for maximum swelling of the materials. After this period, the initial wet weight (Wi) of the hydrogels was determined by gently removing surface moisture using absorbent paper, with samples placed for 10 min on each side at 37°C, followed by weighing on a microprecision balance (Mettler Toledo XS105 DualRange; Columbus, OH, USA). The different material formulations were immersed in PBS at 37°C, and at each evaluation time point (1, 3, 7, 14, 21, and 28 days), the wet weight (Ww) of the samples was measured using the procedure described above. The PBS was refreshed weekly during the experiment. The percentage of degradability (DG) was calculated using the following equation:

$$DG\ (\%) = (Ww - Wi) / Wi \times 100.$$

**Swelling degree assay:** Hydrogels from the experimental groups were prepared (n=5) under aseptic conditions, as previously described. The samples were then distributed into 48-well plates and incubated in 1× PBS (pH 7.0) at 37°C for 24 h to achieve maximum swelling of the materials. After this period, excess water was carefully removed using absorbent paper for 5 min on each side, the mass effectively extruded. For the dimensional stability assay, 1 mL of each hydrogel was deposited in a and the Wi of the hydrogels was recorded using a microprecision analytical balance. At predetermined time points (6, 12, and 24 h), the samples were transferred to Eppendorf tubes and frozen overnight at −20°C, followed by freezing at −80°C for 24 h, and subsequently lyophilized at 52°C for 24 h. The lyophilized samples were weighed again using a microprecision analytical balance to obtain the dry weight (Wd) of the hydrogels. The swelling degree (SD) was calculated using the formula:

$$SD\ (\%) = (Wi - Wd) / Wd \times 100$$ [25]

**Compressive modulus test:** The mechanical compression test was performed to evaluate the mechanical strengths and compressive moduli of the samples. For this purpose, samples from each group (n=11) were prepared and subjected to testing using a mechanical testing machine (Digital Line, EMIC, Equipamentos de Ensaio Ltda., São José dos Pinhais, PR, Brazil) equipped with a load cell having a maximum capacity of 200 N (20.4 kgf). The test was conducted at room temperature at a compression rate of 1000 mm/min, until the sample fractured. Compression movements were initiated using a computerized program (Tesc-Test Script; EMIC). Maximum load values (N) were divided by the cross-sectional area of each specimen ($mm^2$) to obtain stress values in megapascals (MPa). The compressive modulus was then calculated from the stress-strain curve, where stress ($\sigma = F/A$) was obtained by dividing the applied force (F) by the cross-sectional area (A), and strain ($\varepsilon = \Delta L/L_0$) was calculated by dividing the displacement ($\Delta L$) by the initial height of the sample ($L_0$). The compressive modulus (E_c) was determined as the slope of the initial linear region of the stress-strain curve ($E_c = \Delta\sigma / \Delta\varepsilon$), corresponding to the elastic behavior of the material.

**Injectability and dimensional stability:** The injectability and dimensional stability tests were conducted to evaluate the behavior of the materials during the extrusion process and after photopolymerization. For this purpose, an extrusion printer (Educational Starter, 3D Biotechnologies Solutions, Campinas, SP, Brazil) was configured to allow controlled deposition of the bioinks with a linear displacement of 5 mm. The hydrogels were diluted and maintained at 37°C to simulate physiological conditions. Empty 10-mL syringes were initially weighed and then weighed again after being filled with the hydrogels. The containers used to collect the extruded material were preweighed. Five extrusions were performed for each experimental group, and the containers were weighed after each extrusion to determine separate container and subjected to dimensional analysis using digital calipers. The measurements were performed

10.57647/pibm.2025.1403.18

at two temperatures: 37°C (physiological condition) and 20°C (room temperature). Subsequently, the hydrogels were photopolymerized under standardized conditions and new dimensional measurements were performed, accompanied by photographic records to document the changes.

**Printability assay:** The 3D-printed hydrogel scaffolds were fabricated using an extrusion-based bioprinter (Educational Starter). Printing was performed at room (22°C) and hydrogel temperature of (25°C). The printing parameters were set to a speed of 70 mm/s and flow rate of 150 µL/min, using a 27G stainless steel blunt needle with an inner diameter of 380 µm. Each printed layer was immediately photocrosslinked using a 405-nm LED light source integrated into the bioprinter, with a 10-s exposure per layer. The pore architecture of the hydrogel scaffolds was modulated by adjusting the internal infill density using Repetier–Host software (Hot-World GmbH & Co. KG, Willich, Germany). The final constructs were printed in a quadrangular format with dimensions of 2 × 2 × 0.5 cm and an 80% grid infill. To evaluate the accuracy of the printed scaffolds, transparent resin blocks (ABS-Like Resin Pro 2 Clear, Anycubic, Shenzhen, China), containing a central square defect as the cavity for scaffold fitting (2 × 2 x 0.5 cm) were fabricated using an MSLA printer (Elegoo Saturn 3 Ultra, Elegoo, Shenzhen, China). As described above, hydrogels were printed, stained with Rhodamine B, and positioned within the defect site. The assembled constructs were imaged to qualitatively assess scaffold adaptation and geometric fidelity.

**Cell culture onto hydrogels:** The MC3T3-E1 cell line (ATCC CRL-2593) was chosen for this study as a pre-osteoblast model isolated from mouse calvaria. This cell line has been widely used to evaluate the potential of biomaterials to induce osteogenic differentiation in vitro. Cells were cultured in complete culture medium (α-MEM, Minimum Essential Medium Eagle Alpha, Gibco, Invitrogen), supplemented with 10% fetal bovine serum (FBS) and 1% antibiotic-antimycotic (Gibco, Invitrogen). For biological assays, GelMA samples were prepared as injections and photopolymerized under completely aseptic conditions in 96-well plates, as previously described. Cells (1 x $10^4$) were seeded in a single drop in each well followed by a 30-min incubation at 37°C in an environment with 5% $CO_2$. Thereafter, the constructs were cultured in 200 µL of culture medium up to 14 days.

**Monitoring cell viability:** Cell viability was tested using the Live/Dead assay at 1, 3, 7, and 14 days (n=3). At each time-point, the constructs were washed with PBS and incubated for 10 min in α-MEM without FBS, supplemented with Calcein AM and Ethidium Homodimer-1 (Live/Dead cell viability/cytotoxicity kit; Invitrogen) at 1:1000 concentration. After incubation, the cells were analyzed under a fluorescence microscope (EVOS FLoid Cell Imaging Station; Invitrogen) to detect viable (green-stained, Calcein AM positive) and non-viable (red-stained, Ethidium Homodimer-1 positive) cells. For nuclear staining, Hoechst dye (1:10,000, Life Technologies, Carlsbad, CA, USA) was used to stain the nuclei blue. The toxic concentrations were excluded from the assays.

**Cell proliferation:** The Alamar Blue assay (Life Technologies) was used to assess the metabolic activity of the cells after 1, 3, 7, and 14 days of culture (n=6). The samples were incubated for 4 h at 37°C and 5% $CO_2$ in α-MEM without FBS, containing the Alamar Blue reagent at a 10:1 ratio. The supernatant was collected, analyzed for fluorescence, and measured at 540 nm excitation and 590 nm emission wavelengths (Synergy H1, Biotek, Winooski, USA). The average fluorescence value obtained for the negative control group (cells cultured on GelMA without oxides) was considered 100% of cell metabolism.

**Mineralized matrix deposition:** The direct contact assay was performed by culturing the cell/hydrogel constructs for 7 and 14 days (n=6) in an osteogenic medium (50 µg/mL ascorbic acid and 5 mM β-glycerophosphate; Sigma-Aldrich) as previously described. At each time point, the hydrogel samples were fixed with 70% ethanol for 1 h at room temperature, washed with PBS, and incubated with Alizarin Red solution (40 mM, pH 4.2; Sigma-Aldrich) for 15 min under agitation. Subsequently, each hydrogel sample was washed five times with PBS and a solution of cetylpyridinium chloride (10 mM, pH 7.0; Sigma-Aldrich) was applied for 15 min to dissolve the staining. The absorbance of the resulting solution was measured at 560 nm (Synergy H1; BioTek). Hydrogels without cell culture were used as background controls for each formulation (n=3). An indirect contact assay was conducted to assess the bioactive potential of hydrogels at different distances. For this purpose, 5 × $10^4$ MC3T3-E1 cells were seeded in each well of sterilized 24-well plates. After removing the original membranes in the modified transwell inserts (CellStar, Greiner), Hydrogel samples were inserted and secured to the lateral walls using polydimethylsiloxane. Twenty-four hours after cell seeding, the hydrogel-transwell assemblies were placed into the wells, ensuring that the hydrogel surface remained in close proximity to the underlying cell monolayer without establishing direct physical contact. Two weeks later, Alizarin red staining was performed as previously described. For both assays, the cells in the plain GelMA group were considered to have 100% mineralized matrix deposition.

**Collagen expression:** The collagen expression was analyzed in the culture medium in which the samples were

10.57647/pibm.2025.1403.18

maintained on days 3, 7, and 14 (n=6). The Soluble Collagen Quantification Assay Kit (CS0006; Sigma-Aldrich) was used. The kit recommended preparing a standard curve during the assay and samples were analyzed in duplicate in a 96-well plate. At each time-point, 80 µL of the supernatant was collected in duplicate after culture medium centrifugation at 10,000 x g for 15 min at 4°C. The collected volume was then transferred to the plate, and each well received 20 µL of the diluted Digest Enzyme (1x), followed by incubation for 1 h at 37°C. After this period, 75 µL of the Probe solution was added and the samples were incubated for an additional 5 min at 37°C. Finally, 25 µL of the Development Solution (dissolved in 1x) was added to each well and the samples were incubated for 10 min under the same conditions. The fluorescence of the groups was then analyzed using a Synergy microplate reader and measured at excitation and emission wavelengths of 375 nm and 465 nm, respectively.

**Statistical analysis:** Three independent experiments were conducted for data collection and analysis. All data were analyzed using the Prism 10 software (GraphPad Software, San Diego, CA, USA). One-way or two-way analysis of variance (ANOVA) was performed as appropriate, followed by Tukey's post-hoc test to determine statistically significant differences between groups. Statistical significance was set at $p < 0.05$.

## 3. Results

**Dose-response assay:** Higher concentrations of both oxides (1%, 0.1%, and 0.075%) resulted in the highest amount of cell death, in a dose-dependent manner (Figure 1). In contrast, the lowest concentrations of both oxides (0.05% and 0.025%) enhanced cell viability. Considering these findings, subsequent experiments were performed with only 0.05% (w/v) and 0.025% (w/v) oxide concentrations, using pure GelMA as a control.

**Physico-chemical characterization:** Figure 2a presents the SEM images of the biomaterials, indicating that in the presence of oxides, a highly porous structure was obtained. Figure 2b shows FTIR spectra. The hydrogels containing MgO exhibited characteristic bands below 1000 $cm^{-1}$ (873, 670, 580 $cm^{-1}$), which can be associated with the absorption and complexation of MgO within the GelMA structure, being more evident in the 0.05% MgO GelMA hydrogel [26]. The bands observed in the 550–670 $cm^{-1}$ range have been confirmed to correspond to Mg–O stretching vibrations [27].

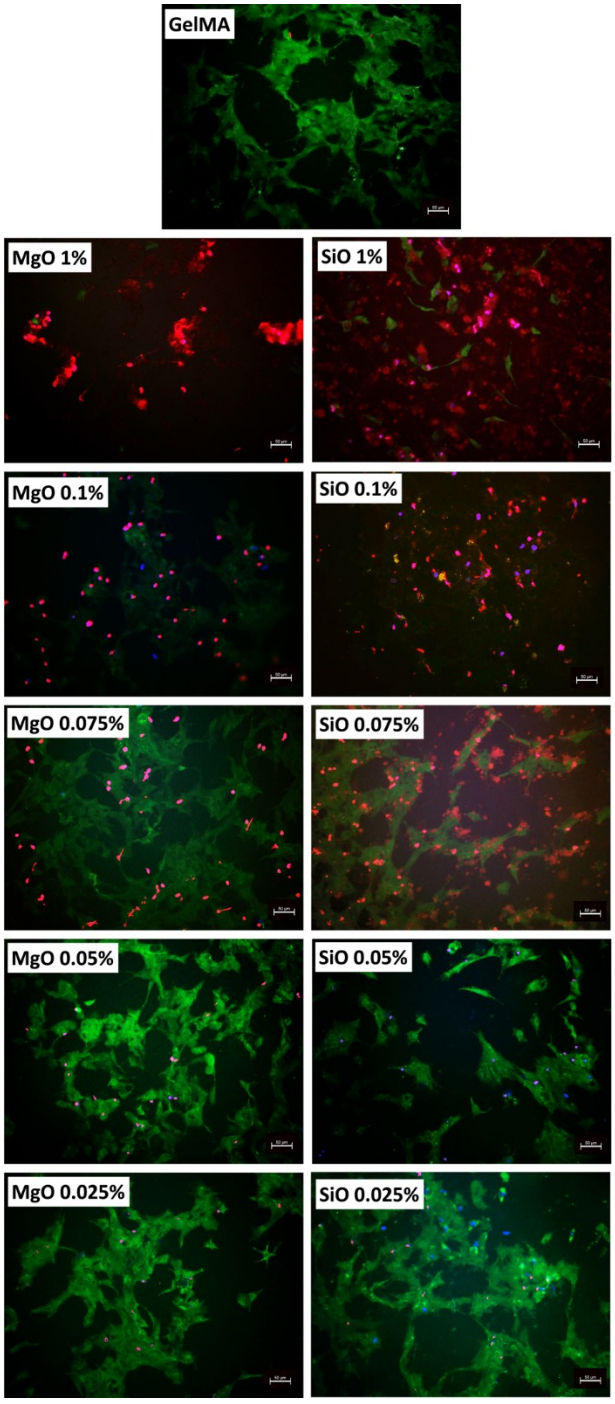


**Figure 1.** Dose-response assay. Panel of Live/Dead assay results for the dose-response analysis. Representative fluorescence images (20× magnification) of GelMA hydrogels containing varying concentrations of MgO and $SiO_2$ nanoparticles after 24 h of cell culture. Green fluorescence indicates viable cells (Calcein-AM), red fluorescence indicates dead cells (Ethidium Homodimer-1), and blue fluorescence indicates nuclear staining (Hoechst). Notable cell viability was observed when the two lowest concentrations of both oxides (0.05% and 0.025%) were used. The two highest concentrations of both oxides (1% and 0.1%) caused the most intense cell death. Cells exposed to 0.075% of both mineral nanoparticles exhibited equilibrium between viability and death. GelMA, methacrylated gelatin

10.57647/pibm.2025.1403.18

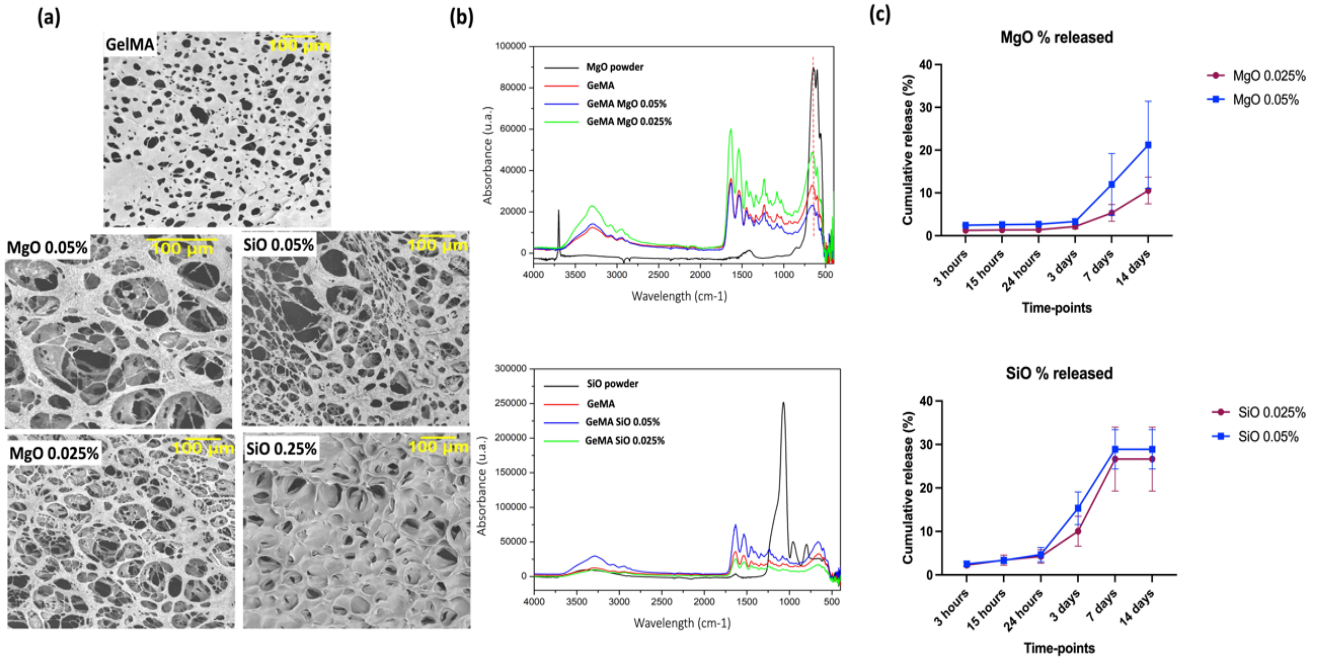


**Figure 2.** Physico-chemical characterization assay. (a) Scanning electron microscope (SEM) images of the hydrogel formulations at 250× magnification, highlighting surface morphology and pore architecture. (b) Fourier-transform infrared spectroscopy (FTIR) spectra of GelMA hydrogels enriched with MgO and $SiO_2$, showing characteristic absorption bands related to oxide complexation. (c) Cumulative release profiles of MgO and $SiO_2$ over time, indicating release kinetics for each composition. GelMA, methacrylated gelatin

The SiO2 powder exhibited a granular morphology, with a more intense spectrum than that of the other groups. Despite this, a subtle peak can be observed in the region around 1643 $cm^{-1}$, attributed to the O–H group, as well as a band at 1094 $cm^{-1}$, corresponding to the Si–O–Si stretching frequency, confirming the discrete complexation of SiO2 within the GelMA structure [28]. In the oxide release assay (Figure 2c), a minimal release of the total MgO incorporated into the GelMA matrix occurred at early time points (3 h, 15 h, 24 h, and 3 days). Approximately 12% and 21% oxide release was observed in the 0.025% MgO group after 7 and 14 days, respectively. However, only 4% and 9% oxide release occurred in the 0.05% MgO group over the same time points.

An oxide release profile similar to that of MgO was observed for groups containing SiO2 at both concentrations during the initial evaluation period. Nevertheless, a more pronounced release occurred after 3 days, with percentages of approximately 9% and 15% for 0.05% SiO2 and 0.025%SiO2, respectively. From day 7 onwards, controlled release of SiO2 was achieved in both groups, with similar percentages for 0.025% (29%) and 0.05% SiO2 (27%). The stability of the GelMA-based hydrogels with and without the incorporation of MgO and SiO2 nanoparticles was evaluated under hydrolytic and enzymatic conditions. In PBS (Figure 3a), all groups maintained their initial mass over the 28-day period, with only minor variations within the standard deviation range, indicating that the addition of MgO or SiO2 at both concentrations (0.025% and 0.05%) did not affect the hydrolytic stability of the hydrogels. Conversely, in the presence of collagenase (Figure 3b), all groups exhibited progressive mass loss, reaching complete degradation by day 14. No significant differences were observed between the pure GelMA and nanoparticle-containing groups, suggesting that MgO and SiO2 incorporation did not alter the enzymatic degradation kinetics. The swelling behaviors of the hydrogels are shown in Figure 3c. The pure GelMA scaffolds exhibited the lowest swelling ratio, whereas the inclusion of MgO and SiO2 significantly increased the water uptake. This effect suggests that the incorporation of nanoparticles enhances the ability of the hydrogel network to absorb water, likely by increasing the hydrophilicity or inducing structural rearrangements within the polymeric matrix.

The compressive moduli of different groups are shown in Figure 3d. All the hydrogels displayed comparable mechanical properties, with mean values ranging from 0.4 to 0.5 MPa. Although GelMA exhibited a slight tendency toward higher stiffness, no statistically significant differences were detected among the groups. These findings indicate that the incorporation of MgO and SiO2 nanoparticles does not compromise the mechanical performance of the GelMA hydrogels under compressive stress.

10.57647/pibm.2025.1403.18

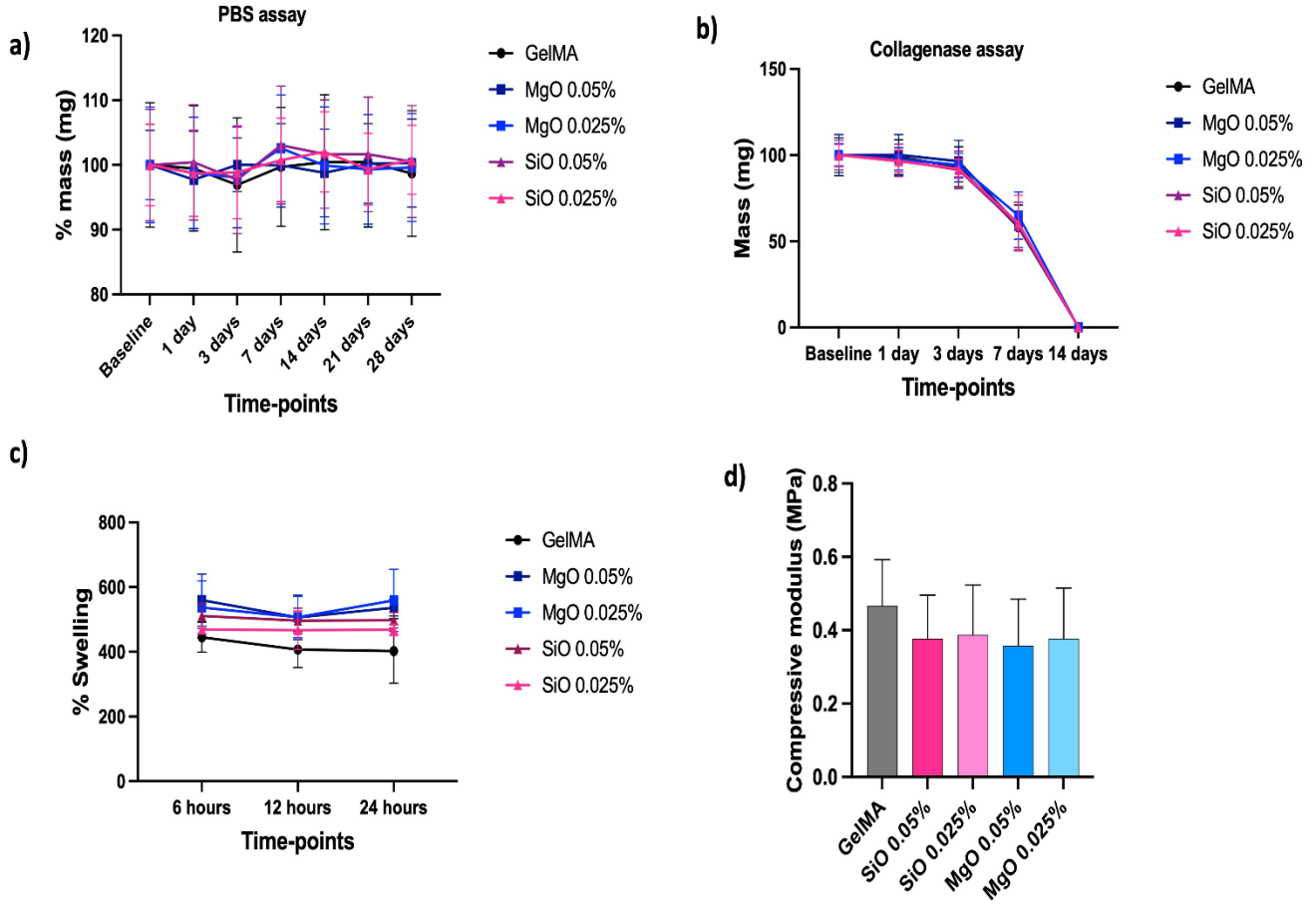


**Figure 3.** Physico-chemical characterization of GelMA-based hydrogels with and without MgO and $SiO_2$ nanoparticles. (a) Hydrolytic degradation in PBS, showing stable mass over 28 days for all groups. (b) Enzymatic degradation in collagenase, with progressive mass loss and complete degradation by day 14, independent of nanoparticle incorporation. (c) Swelling ratio, where MgO- and SiO2-containing groups exhibited significantly higher water uptake compared with that of pure GelMA. (d) Compressive modulus, showing comparable mechanical properties across all groups, with no significant differences between formulations. GelMA, methacrylated gelatin; PBS, phosphate-buffered saline

**Injectability and dimensional stability:** The injectability assay demonstrated that the extrusion of the bioinks varied according to the composition of the formulations (Figure 4a). Pure GelMA exhibited an intermediate extruded mass (~0.55 mg), whereas the addition of 0.05% MgO resulted in comparable performance without impairing injectability. In contrast, the formulation containing 0.025% MgO presented the lowest extruded mass, suggesting a greater resistance to flow.

Bioinks containing $SiO_2$ showed distinct behaviors: at 0.05% concentration, a slight reduction was observed compared with that in the control, while at 0.025% the extrudability was superior, approaching the values obtained for 0.05% MgO (Figure 4b). Overall, these results indicate that the incorporation of metal oxides did not compromise the injectability of the bioinks, with 0.025% MgO being the only exception, showing a less favorable behavior. In the volumetric analysis (Figure 4a), all the bioinks underwent shrinkage after photopolymerization, albeit to different degrees. Pure GelMA exhibited the greatest contraction, decreasing from approximately 2.0 to 1.0 $mm^3$, highlighting its dimensional instability.

The presence of MgO conferred improved stability, particularly at 0.025% concentration, where the initial volume of approximately 3.0 $mm^3$ was maintained at approximately 2.3 $mm^3$ after curing, indicating lower relative shrinkage. MgO at 0.05% also reduced contraction, maintaining volumes from approximately 2.5 $mm^3$ before to 2.0 $mm^3$ after photopolymerization. For $SiO_2$, the 0.05% concentration resulted in the highest proportional volume loss, decreasing from 1.7 to 1.5 $mm^3$. Conversely, the formulation with 0.025% $SiO_2$ exhibited a more balanced behavior, reducing from 2.5 to 2.0 $mm^3$. These findings demonstrate that the addition of MgO and $SiO_2$ can contribute to improved dimensional stability of the bioinks, with particular emphasis on the 0.025% MgO formulation, which exhibited the lowest volumetric shrinkage after crosslinking (Figure 4c).

10.57647/pibm.2025.1403.18

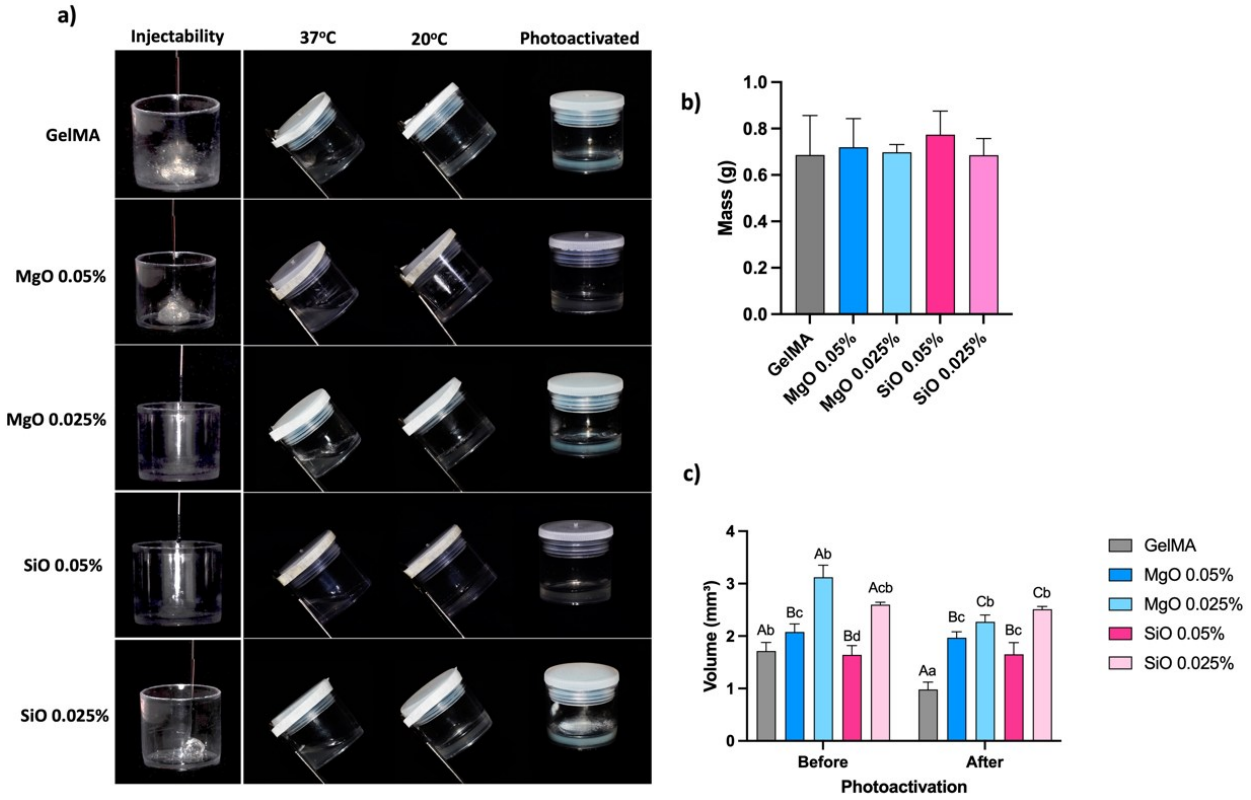


**Figure 4.** Evaluation of the injectability, thermal behavior, and photo-crosslinking capacity of GelMA-based hydrogels containing different concentrations of MgO and $SiO_2$ nanoparticles. (a) Representative images showing the injectability and physical behavior of the hydrogels at 37°C and 20°C, and after photoactivation. (b) Hydrogel mass measured after photo-crosslinking, indicating no significant material loss (likely n=5, according to the injectability method, mean ± SD). (c) Hydrogel volume before and after photoactivation, demonstrating volumetric stability across different formulations. Different letters indicate statistically significant differences between groups ($p < 0.05$). GelMA, methacrylated gelatin

**Printability and accuracy:** Representative images of the 3D-printed scaffolds are shown in Figure 5a. All the formulations, including pure GelMA and GelMA containing MgO or SiO2 nanoparticles, were successfully printed with a defined architecture. The scaffolds demonstrated adequate structural fidelity with multiple stacked layers and a consistent pore distribution. When fitted to the defect model, all groups exhibited good macroscopic adaptation, indicating that the presence of MgO or SiO2 did not compromise their ability to conform to the defect geometry. Quantitative analysis of the pore morphology is presented in Figure 5b and 5c. Pore area measurements revealed significant differences between the groups. Pure GelMA exhibited larger mean pore areas, whereas the addition of MgO (both 0.05% and 0.025%) resulted in a marked reduction in the pore area ($p < 0.05$). Conversely, SiO2 incorporation, particularly at 0.025%, maintained pore sizes closer to those of GelMA, suggesting a less pronounced influence on pore geometry. Similar trends were observed for the pore perimeter (Figure 5c), where MgO-containing scaffolds displayed significantly lower values than that of GelMA, whereas the SiO groups remained statistically comparable to the control. These findings suggest that MgO may alter the rheological or cross-linking characteristics of the precursor solution, leading to smaller pore dimensions, whereas $SiO_2$ exerts minimal influence on the print fidelity.

**Biological characterization:** The Live/Dead assay (Figure 6a) confirmed the sustained presence of viable cells on the surface of the GelMA hydrogels functionalized with metal oxides at different concentrations over a 14-day period. The Alamar Blue assay (Figure 6b) revealed a progressive increase in cellular metabolic activity over time for all tested formulations, indirectly indicating enhanced cell proliferation. At days 3, 7, and 14, cells in all oxide-functionalized GelMA groups exhibited significantly higher metabolic activity than that of the plain GelMA control. At 14 days, the cells seeded onto GelMA containing 0.05% MgO showed higher metabolism than those in the SiO2-containing groups. Figure 6c demonstrates that collagen expression was upregulated in cells seeded on all oxide-containing GelMA formulations after a 7 day-period compared with that in the plain GelMA control. Notably, the 0.025% MgO and 0.05% SiO2 groups maintained elevated collagen expression levels on day 14.

10.57647/pibm.2025.1403.18

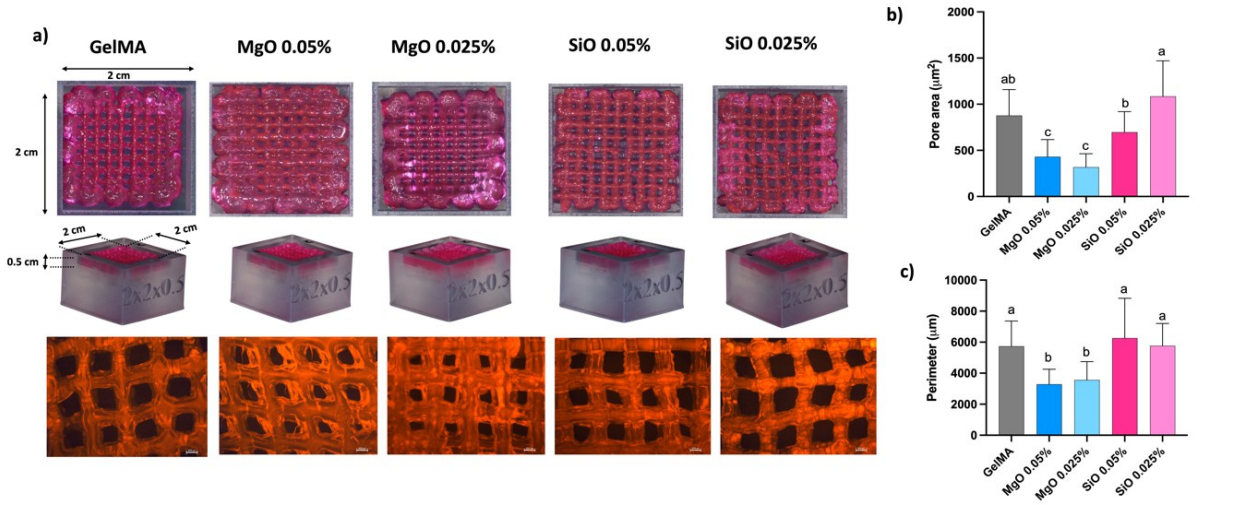


**Figure 5.** Printability and defect adaptation of GelMA-based hydrogels. (a) Representative images of printed scaffolds fitted into defect models, showing adequate adaptation across all groups. (b) Quantification of pore area, showing reduced values in MgO-containing scaffolds compared with that of GelMA and SiO2 groups. (c) Pore perimeter measurements, with MgO scaffolds displaying significantly lower values and $SiO_2$ remaining comparable to GelMA. GelMA, methacrylated gelatin

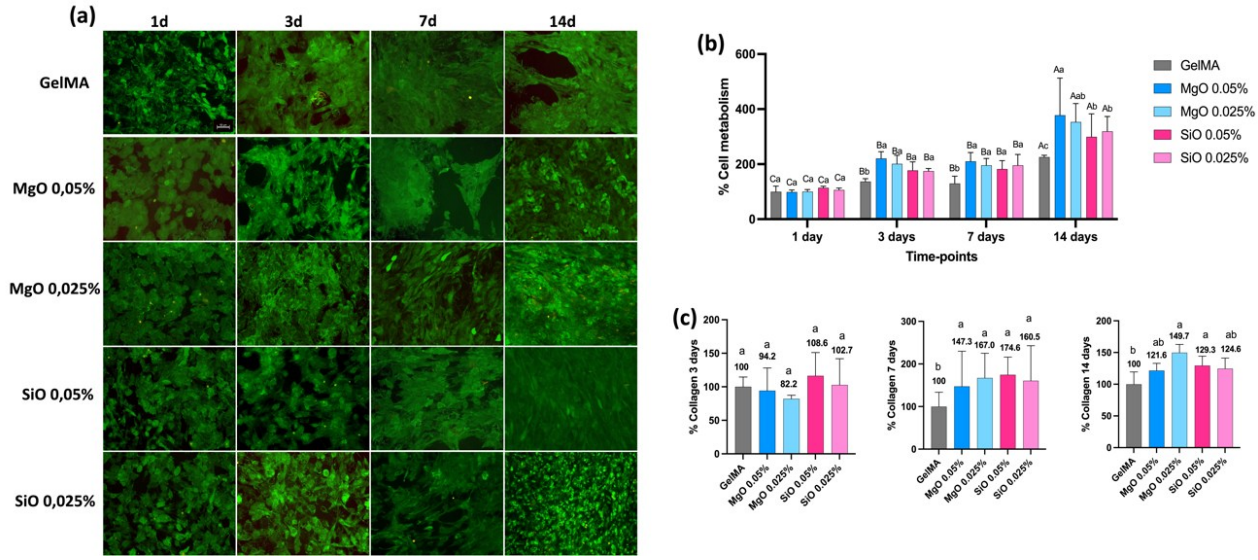


**Figure 6.** Biological characterization. (a) Live/Dead assay. Representative fluorescence images (20× magnification) of GelMA hydrogels containing or not containing different concentrations of MgO and SiO2. Green and red staining shows viable and dead cells, respectively. (b) Alamar Blue assay. The bar graph demonstrates the mean values ± standard deviations of cellular metabolic activity. (c) Soluble collagen assay. The bar graph shows the mean values ± standard deviations of collagen expression at 3, 7, and 14 days. (b, c) Uppercase letters denote statistically significant differences between timepoints within the same group; lowercase letters denote significant differences between groups at the same timepoint (one-way ANOVA followed by Tukey's post hoc test; $p<0.05$). GelMA, methacrylated gelatin

**Mineralized matrix deposition:** The direct contact assay (Figure 7a) demonstrated pronounced bioactive potential for all GelMA formulations containing metal oxides, which presented greater mineralized matrix deposition than that of the control group (plain GelMA). At 7 days (Figure 7b), no statistical differences were observed among the oxide-functionalized groups. However, by day 14 (Figure 7c), the GelMA formulations containing 0.05% MgO and 0.05% SiO2 showed significantly higher mineralized matrix deposition than that of the other experimental groups. Specifically, 0.05% GelMA-MgO and 0.05% GelMA-SiO2 exhibited 3.9-fold and 4.3-fold increases, respectively, compared with that in plain GelMA. Digital images of the samples corroborated these results (Figure 7d). The indirect contact assay (Figure 7e) further confirmed the bioactive potential of all oxide-containing formulations, as evidenced by greater deposition of the mineralized matrix compared with that in the control group (plain GelMA). Among the tested groups, the 0.05% MgO and 0.05% SiO2 formulations demonstrated the highest levels of matrix mineralization. However, statistically significant differences among the oxide-functionalized groups were observed only when these formulations were compared with the SiO2 0.025% group. Images of mineralized nodule formation corroborated these results (Figure 7f).

10.57647/pibm.2025.1403.18

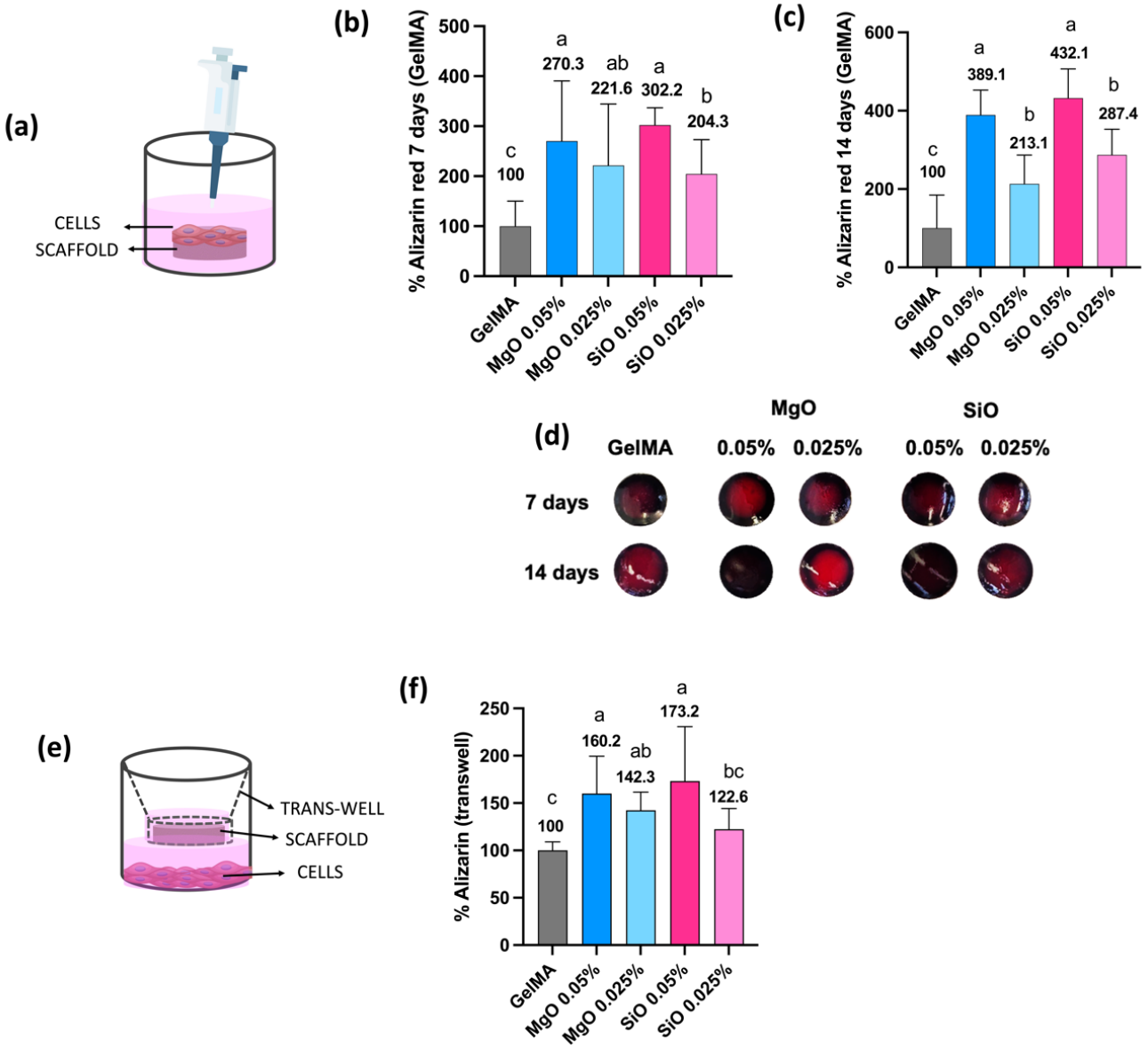


**Figure 7.** Alizarin red assay. (a) Schematic of direct contact assay. (b, c) Bar graphs representing Alizarin red staining of hydrogels seeded with MC3T3 cells at 7 and 14 days, respectively. (d) Digital images of GelMA stained with Alizarin red. (e) Schematics of indirect contact assay. (f) Bar graph of mineralized matrix deposition by cells co-cultured with hydrogels at 14 days. Data are presented as mean values ± standard deviations. Uppercase letters indicate statistically significant differences between timepoints within the same group; lowercase letters indicate significant differences between groups at the same timepoint (one-way ANOVA followed by Tukey's post hoc test, $p < 0.05$). GelMA, methacrylated gelatin

## 4. Discussion

GelMA is a cost-effective and readily accessible material with adequate biocompatibility [2]. This hydrogel plays a critical role in maintaining a viable and moist environment at the interface of critically sized bone defects, facilitating gas exchange, removing excess exudates, and promoting cellular infiltration and integration [29]. Furthermore, the combination of GelMA with other compounds can improve its physical, morphological, and biological properties, allowing the preparation of specific formulations based on the clinical therapy requirements [30]. In the present study, bioactive oxides were incorporated into a GelMA hydrogel to develop a bioactive product for mineralized tissue regeneration. A GelMA solution was initially prepared at a 15% (w/v) concentration with 0.075% (w/v) LAP as the photoinitiator, following the protocol previously described by [21]. This formulation resulted in a stable and biocompatible network upon 30-s photopolymerization using polywave LED light device commonly available in dental offices. Oxide incorporation was conducted as outlined by [22] to ensure effective dispersion of the oxides throughout the hydrogel. The oxides were then dispersed

in a BSA-ethanol solution before being incorporated into a GelMA solution.

A dose-response assay was conducted to identify the biocompatible concentrations of oxides for incorporation into GelMA, and 0.05% and 0.025% (w/v) were selected. The live/dead assay showed that viable pre-osteoblasts attached and stretched to the hydrogel structure 14 days after seeding these cells. SEM analysis confirmed the absence of oxide aggregation at these low concentrations, with the particles uniformly distributed throughout the hydrogel matrix and exhibiting an increased porous architecture. Therefore, the incorporation method used in this study facilitated optimal functionalization of the oxides within the GelMA matrix, effectively preventing aggregation and resulting in a uniform hydrogel with a well-organized pore network.

The increase in GelMA porosity mediated by oxide incorporation may occur through the following mechanisms: (i) enhanced local viscosity arising from particle-polymer interactions, which can influence pore formation and stabilization during lyophilization or extrusion; (ii) potential alterations in crosslinking kinetics, as MgO may interact with GelMA functional groups; and (iii) light scattering effects during photocrosslinking, which can affect local polymerization (Jalilinejad et al., 2025; Mei et al., 2022). High-porosity bioproducts facilitate cellular infiltration, proliferation, and neotissue formation [31; 32]. In addition to the improved porous architecture, the GelMA hydrogel provided a controlled release profile for the incorporated oxides, thereby preventing burst release. According to the results obtained in the present study, the release of oxides from biomaterials occurred in a uniform and gradual manner over a period of 14 days.

Physical characterization of GelMA using FTIR spectroscopy confirmed the successful functionalization of gelatin with methacrylate groups, as evidenced by additional ester and vinyl absorption bands overlapping with the amide region [33]. The FTIR analysis of GelMA functionalized with oxides was consistent with the findings of [25, 26] , as MgO exhibited results consistent with its absorption and complexation within the GelMA structure, along with its characteristic stretching vibrations. Similarly, [27] attributed the observed results for SiO2 to its stretching frequency, which explained its discrete complexation within the GelMA matrix. Hydrolytic stability was maintained across all groups for 28 days in PBS, while complete enzymatic degradation occurred within 14 days in collagenase, consistent with the enzymatic nature of GelMA resorption and unaffected by MgO or $SiO_2$ incorporation [34; 35]. Nanoparticle role in cell proliferation, differentiation, and maintenance of an osteoblastic phenotype in resident cells, which may addition increased the swelling ratio, likely due to enhanced hydrophilicity and network reorganization, favoring nutrient diffusion but requiring a balance to avoid structural compromise [2]. The compressive modulus (0.4–0.5 MPa) remained comparable to that of pure GelMA, which may be a consequence of the low concentration of incorporated nanoparticles, as previously described [36, 21].

In terms of physical characterization, viscosity behavior was inferred from injectability and dimensional stability; however, quantitative rheological measurements were not performed. The injectability assay indicated that incorporating MgO and $SiO_2$ into GelMA hydrogels did not impair extrusion performance; formulations containing 0.025% $SiO_2$ and 0.05% MgO showed maintained or even improved extruded mass compared with that of pure GelMA. This behavior is consistent with previous reports, in which inorganic nanoparticles acted as rheological fillers, enhancing shear-thinning properties, post-shear recovery, and consequently, nozzle flow and shape fidelity [51; 23; 38; 39]. The literature further supports the positive role of silica- and magnesium-based nanoparticles in improving the printability of GelMA bioinks by promoting particle-matrix interactions and thixotropic microstructures that reduce the extrusion viscosity and favor structural recovery [40-42]. Consistent with these findings, the present study also demonstrated that MgO- and $SiO_2$-containing scaffolds maintained adequate macroscopic adaptation in defect models, confirming that nanoparticle incorporation preserved the ability of the constructs to conform to predefined geometries, an essential design criterion in bone tissue engineering [44, 45].

To investigate the biological potential of the developed bioinks, MC3T3-E1 cells were seeded onto the GelMA structures and cultured in vitro for 14 days. Although this model is suitable for early-stage screening, the absence of human cell models and *in vivo* validation are limitations of the present study. The results demonstrated a pronounced bioactive potential for GelMA formulations containing 0.025% and 0.05% (w/v) MgO or $SiO_2$. Proliferation assays further revealed that cells seeded onto these composites exhibited significantly higher proliferative activity than that of pure GelMA, starting from day 3 of the culture. The enhanced porosity of the biomaterials developed in the present study may have contributed to increased cell proliferation, which was mainly observed for the oxide-functionalized GelMA formulations. [46] reported that the sustained release of bioactive molecules plays a critical

partially explain the positive outcomes observed in the present study using the Alizarin Red assay. Previous

research indicate that upon contact with moist environments, these particles release well-known bioactive ions, $Mg^{2+}$ and $Si^{4+}$, which activate the expression of osteogenic genes [47-49]. The expression of osteogenic genes contributes to mineralization and increased collagen production, as observed in the present study. Upregulation of collagen expression and mineralized matrix deposition occurred when the cells were seeded in direct contact with the hydrogels.

A high bioactive effect was detected at the 0.05% concentration, as a significantly high mineralized matrix deposition was observed after 14 days. This positive effect may be caused by direct cellular interactions with the oxide-enriched GelMA matrix and proosteogenic microenvironment induced by the release of bioactive ions from this biomaterial. The indirect assay further confirmed that the oxides released from the hydrogels in close proximity to the cells were capable of inducing osteoblastic differentiation associated with the deposition and mineralization of the collagen-rich matrix.

Studies have shown that the presence of various forms of magnesium in bone defects stimulates bone regeneration by promoting the proliferation and migration of preosteoblastic cells and accelerating osseointegration [28; 50; 48; 51]. Additionally, [48] demonstrated that MgO induces the expression of genes directly associated with osteogenesis in bone marrow mesenchymal stem cells. [52] and [53] also revealed that silicon activates various mechanisms related to bone regeneration and maintenance of bone tissue health. The authors determined that SiO2 promotes collagen synthesis (mainly type I) and matrix mineralization as well as reduces the number of osteoclasts and enhances DNA synthesis by osteoblasts. Similar to MgO, the authors showed that SiO2 is also capable of increasing osteoblast markers, such as SOD1, Runx2, Sp7, Smad1, Smad5, and type I collagen [53; 52]. These notable data are corroborated by the results obtained in the present study, in which GelMA hydrogels incorporated with both MgO and SiO2 at concentrations of 0.025–0.05% exhibited notable bioactivity on pre-osteoblasts. These oxide-functionalized GelMA hydrogels, which represent a friendly injectable platform for mineralized tissue regeneration, have the advantage of rapid polymerization by LED irradiation, highlighting their potential for various clinical applications, particularly in dentistry.

Therefore, the results obtained in the present investigation indicate that the incorporation of bioactive concentrations of MgO and SiO2 into the GelMA hydrogel allows the development of a bioink with no significant compromise to the physicomechanical performance and printability of the biomaterial. While further investigations are warranted, the incorporation of MgO and SiO2 at low concentrations into GelMA hydrogels may be a promising strategy for obtaining the successful use of biomaterials for bone tissue regeneration. Further investigation is required to confirm the translational potential of the proposed system.

**Ethical Statement**

No experimental procedures involving animal or human models were undertaken in the present study.

## 5. Conclusions

The incorporation of bioactive concentrations of MgO and SiO2 into the GelMA matrix resulted in a bioactive, injectable, printable hydrogel with enhanced porosity and a favorable microenvironment for cell adhesion, proliferation, and differentiation. GelMA containing 0.05% MgO and SiO2 exhibited the highest well-defined osteogenic activity, making it the most promising biomaterial for bone tissue regeneration.

**Authors Contribution**

Lígia Espoliar Corrêa – Conceptualization, Methodology, Investigation, Data Curation, Writing – Original Draft. Ester Alves Ferreira Bordini – Conceptualization, Methodology, Investigation, Data Curation. Vitor de Toledo Stuani – Conceptualization, Methodology, Investigation, Data Curation Larissa Álamo – Methodology, Investigation, Data Curation Ruan Henrique Delmonica Barra – Data Curation, Writing – Original Draft. Erika Soares Bronze-Uhle – Methodology, Investigation, Data Curation. Laura Ferreira Almeida – Methodology, Investigation. Lídia de Oliveira Fernandes – Methodology, Data Curation. Carolina Alves Andrade - Methodology, Data Curation. Juliano Milanezi de Almeida – Conceptualization, Writing – Review & Editing . Carlos Alberto de Souza Costa – Conceptualization, Writing – Review & Editing. Diana Gabriela Soares – Conceptualization, Data Curation, Writing – Review & Editing, Supervision, Project Administration, Funding Acquisition

**Availability of data and materials**

Data is available upon request

**Conflict of interests**

The authors have no relevant financial or non-financial interests to disclose.

**Acknowledgments**

The authors acknowledge and express their gratitude for the support provided by the São Paulo Research Foundation (FAPESP) [grant numbers 2022/05888-9, 2020/15971-5, and 2023/08880-1] and Coordination for the Improvement of Higher Education Personnel (CAPES)[Finance Code 001].

**Declaration of generative AI and AI-assisted technologies in the writing process.**

During the preparation of this work, the authors used ChatGPT 4.0 to improve the readability and language of the manuscript. After using this tool/service, the authors reviewed and edited the content as needed and take full responsibility for the content of the published article.

## References


[1] Han J, Menicanin D, Gronthos S, Bartold PM. Stem cells, tissue engineering and periodental regeneration. Aust Dent J. 2014 Jun;59 Suppl 1:117-30.

[2] Zhao N, Wu Z, Qin L, Guo Z, Li D. Characteristics and Tissue Regeneration Properties of Gingiva-Derived Mesenchymal Stem Cells. Crit Rev Eukaryot Gene Expr. 2015;25(2):135-44.

[3] Zhai Q, Dong Z, Wang W, Li B, Jin Y. Dental stem cell and dental tissue regeneration. Front Med. 2019 Apr;13(2):152-9.

[4] Lee SH, Kang MS, Jeon S, Jo HJ, Hong SW, Kim B, et al. 3D bioprinting of human mesenchymal stem cells-laden hydrogels incorporating MXene for spontaneous osteodifferentiation. Heliyon. 2023 Mar;9(3):e14490.

[5] Karanth D, Song K, Martin ML, Meyer DR, Dolce C, Huang Y, et al. Towards resorbable 3D-printed scaffolds for craniofacial bone regeneration. Orthod Craniofac Res. 2023 Nov;26 Suppl 1:117-25.

[6] Shen M, Wang L, Gao Y, Feng L, Xu C, Li S, et al. 3D bioprinting of in situ vascularized tissue engineered bone for repairing large segmental bone defects. Mater Today Bio. 2022;16:100382

[7] Tao J, Zhu S, Liao X, Wang Y, Zhou N, Li Z, et al. DLP-based bioprinting of void-forming hydrogels for enhanced stem-cell-mediated bone regeneration. Mater Today Bio. 2022;17:100487.

[8] Wang J, Wang X, Liang Z, Lan W, Wei Y, Hu Y, et al. Injectable antibacterial Ag-HA/ GelMA hydrogel for bone tissue engineering. Front Bioeng Biotechnol. 2023 Jun 14;11:1219460.

[9] Liu Z, Li Y, Song H, He J, Li G, Zheng Y, et al. Collagen peptides promote photoaging skin cell repair by activating the TGF-β/Smad pathway and depressing collagen degradation. Food Funct. 2019 Sep 1;10(9):6121-34.

[10] Lin K, Zhang D, Macedo MH, Cui W, Sarmento B, Shen G. Advanced collagen-based biomaterials for regenerative biomedicine. Adv Funct Mater. 2019;29(3):1804943.

[11] Nurilmala M, Darmawan N, Putri EAW, Jacoeb A, Irawadi T. Pangasius fish skin and swim bladder as gelatin sources for hard capsule material. Int J Biomater. 2021;2021:6658002.

[12] Drzewiecki KE, Parmar AS, Gaudet ID, Branch JR, Pike DH, Nanda V, et al. Methacrylation induces rapid, temperature-dependent, reversible self-assembly of type-I collagen. Langmuir. 2014 Sep 23;30(37):11204-11.

[13] Xiao S, Zhao T, Wang J, Wang C, Du J, Ying L, et al. Gelatin Methacrylate (GelMA)-Based Hydrogels for Cell Transplantation: an Effective Strategy for Tissue Engineering. Stem Cell Rev Rep. 2019 Oct;15(5):664-79.

[14] Lee M, Rizzo R, Surman F, Zenobi-Wong M. Guiding Lights: Tissue Bioprinting Using Photoactivated Materials. Chem Rev. 2020 Oct 13;120(19):10950-1027.

[15] Liu T, Weng W, Zhang Y, Sun X, Yang H. Applications of Gelatin Methacryloyl (GelMA) Hydrogels in Microfluidic Technique-Assisted Tissue Engineering. Molecules. 2020 Nov 14;25(22):5305.

[16] Bose S, Fielding G, Tarafder S, Bandyopadhyay A. Understanding of dopant-induced osteogenesis and angiogenesis in calcium phosphate ceramics. Trends Biotechnol. 2013 Oct;31(10):594-605.

[17] Braux J, Velard F, Guillaume C, Bouthors S, Jallot E, Nedelec JM, et al. A new insight into the dissociating effect of strontium on bone resorption and formation. Acta Biomater. 2011 Jun;7(6):2593-603.

[18] Fielding GA, Bandyopadhyay A, Bose S. Effects of silica and zinc oxide doping on mechanical and biological properties of 3D printed tricalcium phosphate tissue engineering scaffolds. Dent Mater. 2012 Feb;28(2):113-22.

[19] Zhang W, Chang Q, Xu L, Li G, Yang G, Ding X, et al. Graphene oxide-copper nanocomposite-coated porous CaP scaffold for vascularized bone regeneration via activation of Hif-1α. Adv Healthc Mater. 2016 Jun;5(11):1299-309.

[20] Pu X, Tong L, Wang X, Liu Q, Chen M, Li X, et al. Bioinspired Hydrogel Anchoring 3DP GelMA/HAp Scaffolds Accelerates Bone Reconstruction. ACS Appl Mater Interfaces. 2022;14(18):20591-602.

[21] Yi S, Liu Q, Luo Z, He JJ, Ma HL, Li W, et al. Micropore-Forming Gelatin Methacryloyl (GelMA) Bioink Toolbox 2.0: Designable Tunability and Adaptability for 3D Bioprinting Applications. Small. 2022 Jun;18(25):e2106357.

[22] Silva ISP, Bordini EAF, Bronze-Uhle ES, et al. Photo-crosslinkable hydrogel incorporated with bone matrix particles for advancements in dentin tissue engineering. J Biomed Mater Res A. 2024 Dec;112(12):2273-88.

[23] Choi E, Kim D, Kang D, Yang GH, Jung B, Yeo M, et al. 3D-printed gelatin methacrylate (GelMA)/silanated silica scaffold assisted by two-stage cooling system for hard tissue regeneration. Regen Biomater. 2021;8(2):rbab001.

[24] Ribeiro JS, Bordini EAF, Ferreira JA, Mei L, Dubey N, Fenno JC, et al. Injectable MMP-Responsive Nanotube-Modified Gelatin Hydrogel for Dental Infection Ablation. ACS Appl Mater Interfaces. 2020 Apr 8;12(14):16006-17.

[25] Bordini EAF, Ferreira JA, Dubey N, Ribeiro JS, de Souza Costa CA, Soares DG, et al. Injectable Multifunctional Drug Delivery System for Hard Tissue Regeneration under Inflammatory Microenvironments. ACS Appl Bio Mater. 2021 Sep 20;4(9):6993-7006.

[26] El-Sawy NM, Raafat AI, Badawy NA, Mohamed AM. Radiation development of pH-responsive (xanthan-acrylic acid)/MgO nanocomposite hydrogels for controlled delivery of methotrexate anticancer drug. Int J Biol Macromol. 2020 Jan 1;142:254-64.

[27] El Fadl FIA, Hegazy DE, Maziad NA, Ghobashy MM. Effect of nano-metal oxides (TiO2, MgO, CaO, and ZnO) on antibacterial property of (PEO/PEC-co-AAm) hydrogel synthesized by gamma irradiation. Int J Biol Macromol. 2023 Oct 1;250:126248.

[28] Minisha S, Gopinath A, Mukherjee S, Srinivasan P, Madhan B, Shanmugam G. Impact of SiO2 nanoparticles on the structure and property of type I collagen in three different forms. Spectrochim Acta A Mol Biomol Spectrosc. 2024 Jan 5;304:123520.

[29] Dubey N, Ferreira JA, Daghrery A, Aytac Z, Malda J, Bhaduri SB, et al. Highly tunable bioactive fiber-reinforced hydrogel for guided bone regeneration. Acta Biomater. 2020 Sep 1;113:164-76.

[30] Chen Y, Zheng Z, Zhou R, Zhang H, Chen C, Xiong Z, et al. Developing a Strontium-Releasing Graphene Oxide-/Collagen-Based Organic-Inorganic Nanobiocomposite for Large Bone Defect Regeneration via MAPK Signaling Pathway. ACS Appl Mater Interfaces. 2019 May 1;11(17):15986-97.

[31] Cristallini C, Barbani N, Bianchi S, Maltini S, Baldassare A, Ishak R, et al. Assessing two-way interactions between cells and inorganic nanoparticles. J Mater Sci Mater Med. 2019;31(1):1.

[32] Fini M, Giardino R, Borsari V, Torricelli P, Rimondini L, Giavaresi G, et al. In vitro behaviour of osteoblasts cultured on orthopaedic biomaterials with different surface roughness, uncoated and fluorohydroxyapatite-coated, relative to the in vivo osteointegration rate. Int J Artif Organs. 2003 Jun;26(6):520-8.

[33] Sato M, Webster TJ. Designing orthopedic implant surfaces: harmonization of nanotopographical and chemical aspects. Nanomedicine (Lond). 2006 Sep;1(3):351-4.

[34] Loessner D, Meinert C, Kaemmerer E, Martine LC, Yue K, Levett PA, et al. Functionalization, preparation and use of cell-laden gelatin methacryloyl-based hydrogels as modular tissue culture platforms. Nat Protoc. 2016 Apr;11(4):727-46.

[35] Van Den Bulcke AI, Bogdanowicz D, De Rooze N, Schacht E, Cornelissen M, Berghmans H. Structural and rheological properties of methacrylamide modified gelatin hydrogels. Biomacromolecules. 2000 Spring;1(1):31-8.

[36] Yue K, Trujillo-de Santiago G, Alvarez MM, Tamayol A, Annabi N, Khademhosseini A. Synthesis, properties, and biomedical applications of gelatin methacryloyl (GelMA) hydrogels. Biomaterials. 2015 Dec;73:254-71.

[37] Ouyang L, Armstrong JPK, Chen Q, Lin Y, Stevens MM. Void-free 3D Bioprinting for In-situ Endothelialization and Microfluidic Perfusion. Adv Funct Mater. 2019;30(1):1908349.

[38] Tao Z, Yuan Z, Zhou D, Qin L, Xiao L, Zhang S, et al. Fabrication of magnesium-doped porous polylactic acid microsphere for bone regeneration. Biomater Transl. 2023 Dec 28;4(4):280-90.

[39] Zhu Y, Yu X, Liu H, Li J, Gholipourmalekabadi M, Lin K, et al. Strategies of functionalized GelMA-based bioinks for bone regeneration: Recent advances and future perspectives. Bioact Mater. 2024 Aug;38:346-73.

[40] Schwab A, Levato R, D'Este M, Piluso S, Eglin D, Malda J. Printability and shape fidelity of bioinks in 3D bioprinting. Chem Rev. 2020 Oct 28;120(20):11028-55.

[41] Zandi N, Sani ES, Mostafavi E, Ibrahim DM, Saleh B, Shokrgozar MA, et al. Nanoengineered shear-thinning and bioprintable hydrogel as a versatile platform for biomedical applications. Biomaterials. 2021 Jan;267:120476.

[42] Montanari M, Korkeamäki JT, Campodoni E, Mohamed-Ahmed S, Mustafa K, Sandri M, et al. Effects of Magnesium-Doped Hydroxyapatite Nanoparticles on Bioink Formulation for Bone Tissue Engineering. ACS Appl Bio Mater. 2025 Jan 15;8(1):535-47.

[43] Mouser VH, Melchels FP, Visser J, Dhert WJ, Gawlitta D, Malda J. Yield stress determines bioprintability of hydrogels based on gelatin-methacryloyl and gellan gum for cartilage bioprinting. Biofabrication. 2016;8(3):035003.

[44] Eichholz KF, Freeman FE, Pitacco P, Nulty J, Ahern D, Burdis R, et al. Scaffold microarchitecture regulates angiogenesis and the regeneration of large bone defects. Biofabrication. 2022;14(4):045013.

[45] Du R, Zhao B, Luo K, Wang MX, Yuan Q, Yu LX, et al. Shape Memory Polyester Scaffold Promotes Bone Defect Repair through Enhanced Osteogenic Ability and Mechanical Stability. ACS Appl Mater Interfaces. 2023;15(36):42930-41.

[46] Sikder P, Ferreira JA, Fakhrabadi EA, Kantorski KZ, Liberatore MW, Bottino MC, et al. Bioactive amorphous magnesium phosphate-polyetheretherketone composite filaments for 3D printing. Dent Mater. 2020 Jul;36(7):865-83.

[47] Liu C, Yang G, Zhou M, Zhang X, Wu X, Wu P, et al. Magnesium Ammonium Phosphate Composite Cell-Laden Hydrogel Promotes Osteogenesis and Angiogenesis In Vitro. ACS Omega. 2021 Apr 2;6(14):9449-59.

[48] Ilyas A, Velton M, Shah A, Monte F, Kim HKW, Aswath PB, et al. Rapid Regeneration of Vascularized Bone by Nanofabricated Amorphous Silicon Oxynitrophosphide (SiONP) Overlays. J Biomed Nanotechnol. 2019 Jun 1;15(6):1241-55.

[49] Wu J, Cheng X, Wu J, Chen J, Pei X. The development of magnesium-based biomaterials in bone tissue engineering: A review. J Biomed Mater Res B Appl Biomater. 2024 Jan;112(1):e35326.

[50] Rodella LF, Bonazza V, Labanca M, Lonati C, Rezzani R. A review of the effects of dietary silicon intake on bone homeostasis and regeneration. J Nutr Health Aging. 2014 Nov;18(9):820-6.

[51] Tavares, M. T., Gaspar, V. M., Monteiro, M. V., S Farinha, J. P., Baleizão, C., & Mano, J. F. (2021). GelMA/bioactive silica nanocomposite bioinks for stem cell osteogenic differentiation. Biofabrication, 13(3), 10.1088/1758-5090/abdc86. https://doi.org/10.1088/1758-5090/abdc86